

## Role of frequency dependence of the nonlinearity on a soliton's evolution in photonic crystal fibers

SURAJIT BOSE,<sup>1,\*</sup> OLIVER MELCHERT,<sup>1,2</sup>  STEPHANIE WILLMS,<sup>1,2</sup> IHAR BABUSHKIN,<sup>1,2</sup>   
UWE MORGNER,<sup>1,2</sup> AYHAN DEMIRCAN,<sup>1,2</sup> AND GOVIND P. AGRAWAL<sup>3</sup> 

<sup>1</sup>Institute of Quantum Optics, Leibniz University Hannover, Welfengarten 1, 30167, Hannover, Germany

<sup>2</sup>Cluster of Excellence, PhoenixD, Welfengarten 1, 30167, Hannover, Germany

<sup>3</sup>The Institute of Optics, University of Rochester, Rochester, New York 14627, USA

\*Corresponding author: bose@iqo.uni-hannover.de

Received 3 June 2021; revised 2 July 2021; accepted 11 July 2021; posted 12 July 2021 (Doc. ID 433238); published 6 August 2021

**We reveal the crucial role played by the frequency dependence of the nonlinear parameter on the evolution of femtosecond solitons inside photonic crystal fibers (PCFs). We show that the conventional approach based on the self-steepening effect is not appropriate when such fibers have two zero-dispersion wavelengths, and several higher-order nonlinear terms must be included for realistic modeling of the nonlinear phenomena in PCFs. These terms affect not only the Raman-induced wavelength shift of a soliton but also impact its shedding of dispersive radiation.** © 2021 Optical Society of America

<https://doi.org/10.1364/OL.433238>

The concept of solitons has proved valuable in the context of optical fibers [1] and has found applications in diverse areas such as mode locking of fiber lasers and supercontinuum generation [2]. The formation of solitons requires balancing of the dispersive and nonlinear effects governed by two frequency-dependent parameters,  $\beta(\omega)$  and  $\gamma(\omega)$ , known as the propagation constant and the nonlinear parameter, respectively [1]. The generalized nonlinear Schrödinger equation (GNLSE) incorporates this frequency dependence by expanding the two parameters as a Taylor series around the central frequency of the pulse launched into an optical fiber. For femtosecond pulses, multiple terms in the expansion of  $\beta(\omega)$  are included, but only the first two terms are typically retained for  $\gamma(\omega)$ . The GNLSE also includes the Raman contribution to the fiber's nonlinearity to account for the Raman-induced frequency shift (RIFS) or the soliton self-frequency shift [3].

Both dispersive and nonlinear effects are modified considerably in a photonic crystal fiber (PCF) [4]. Such fibers can be designed to exhibit two zero-dispersion wavelengths (ZDWLs). The RIFS of a soliton is reduced, and even canceled, in the wavelength region of a PCF exhibiting a negative dispersion slope [5]. During such a process, solitons shed some of their energy in the form of nonsolitonic radiation (NSR) or Cherenkov radiation [6]. Other important factors that influence the RIFS include third-order dispersion [1] and self-steepening [7], a nonlinear process related to the first-order term in the Taylor expansion of the nonlinear parameter  $\gamma(\omega)$ . A recent analytical approach to the RIFS has studied its impact [8]. In most past work, the

second and higher-order nonlinear terms in this expansion have been ignored [1,9].

In this Letter, we use numerical simulations to show that the full frequency dependence of  $\gamma(\omega)$  must be accounted for PCFs designed to exhibit two ZDWLs. We also show that sufficiently accurate results can be obtained by including the terms up to third order in the Taylor expansion of the nonlinear parameter  $\gamma(\omega)$ . We study how the higher-order terms dynamically shape the Raman soliton. More specifically, the higher-order terms modify the magnitude of the RIFS of the Raman soliton, which in turn affects its speed and the arrival time at the end of the fiber. Our numerical simulations show that these terms control not only the RIFS of a soliton but also its shedding of dispersive radiation close to the second ZDWL of the fiber.

Propagation of a short optical pulse inside optical fibers is governed by GNLSE, written often in the time domain [1]. To include the full frequency dependence, it is useful to write the GNLSE in the spectral domain as

$$\frac{\partial \tilde{A}_\omega}{\partial z} = i\tilde{\beta}(\omega)\tilde{A}_\omega + i\gamma(\omega)(1 - f_R)\mathcal{F}(A|A|^2) + i f_R\gamma(\omega) \times \mathcal{F}\left(A \int_0^\infty h_R(t')|A(z, t - t')|^2 dt'\right), \quad (1)$$

where  $A(z, t)$  is the pulse envelope in time domain, and  $\tilde{A}_\omega(z) = \mathcal{F}(A)$  is its Fourier transform. Further,  $\tilde{\beta}(\omega) = \beta(\omega) - \beta(\omega_0) - \beta_1(\omega_0)(\omega - \omega_0)$ , and  $h_R$  is the Raman response function [10]. The nonlinear parameter is defined as  $\gamma(\omega) = n_2\omega/[cA_{\text{eff}}(\omega)]$ . Although the frequency dependence of  $n_2$  can be ignored in practice, the strong frequency dependence of  $A_{\text{eff}}(\omega)$  must be included for most PCFs. This was done in [11] with a different modeling method. Only when we replace  $A_{\text{eff}}$  with its value at the central frequency  $\omega_0$  can we write  $\gamma$  in the form  $\gamma(\omega) = \gamma_0 + \gamma_1(\omega - \omega_0)$ , with  $\gamma_1 = \gamma_0/\omega_0$  [1,9].

It is shown that the number of photons remains conserved for Eq. (1) only for the specific value of  $\gamma_1 = \gamma_0/\omega_0$  [12,13], i.e.,  $\gamma(\omega) = \gamma_0\omega/\omega_0$  denoted as  $\gamma_{\text{pc}}$ . As we want to include the full frequency dependence of  $A_{\text{eff}}$  and include the higher-order nonlinear terms, we make use of the so-called photon-conserving GNLSE (pcGNLSE) for our study [13]:

$$\frac{\partial \tilde{A}_\omega}{\partial z} = i\tilde{\beta}(\omega)\tilde{A}_\omega + i\frac{\tilde{\gamma}(\omega)}{2}\mathcal{F}(C^*B^2) + i\frac{\tilde{\gamma}^*(\omega)}{2}\mathcal{F}(B^*C^2) + i f_R \tilde{\gamma}^*(\omega)\mathcal{F}(B \int_0^\infty h_R(t')|B(z, t-t')|^2 dt' - B|B|^2), \quad (2)$$

where  $\tilde{\gamma}(\omega) = \omega \tilde{d}$ ,  $\tilde{B}_\omega = \tilde{d} \tilde{A}_\omega$ ,  $\tilde{C}_\omega = \tilde{d}^* \tilde{A}_\omega$ , and  $\tilde{d} = \sqrt[4]{\gamma(\omega)/\omega}$ . This equation can employ an arbitrary form of  $\gamma(\omega)$ . It has been used recently to study modulation instability [14,15], self-steepening in nonlinear waveguides [16], and the evolution of short solitons in fibers [17,18]. Its soliton-like solutions have also been obtained recently [19]. We solve Eq. (2) numerically using the fourth-order Runge–Kutta method [20].

We focus on a specific class of PCFs exhibiting two ZDWLs with a design given in [21]. Figure 1(a) shows the frequency dependence of the group-velocity dispersion (GVD)  $\beta_2$  and the nonlinear parameter  $\gamma$  calculated for one such fiber. We use these realistic profiles to compute the values of various parameters appearing in the Taylor expansions:

$$\gamma(\omega) = \gamma_0 + \gamma_1(\omega - \omega_0) + \frac{\gamma_2}{2!}(\omega - \omega_0)^2 + \frac{\gamma_3}{3!}(\omega - \omega_0)^3 + \dots, \quad (3)$$

$$\tilde{\beta}(\omega) = \frac{\beta_2}{2!}(\omega - \omega_0)^2 + \frac{\beta_3}{3!}(\omega - \omega_0)^3 + \dots, \quad (4)$$

where  $\gamma_n = \frac{d^n \gamma}{d\omega^n}$  and  $\beta_n = \frac{d^n \beta}{d\omega^n}$  are evaluated at  $\omega = \omega_0$ . We considered up to the sixth-order term in the expansion of  $\gamma(\omega)$  but found that results were sufficiently accurate when we included only terms up to the third-order. In contrast, we needed to include terms up to the 15th order for the GVD expansion.

As we are interested in the evolution of solitons, we solved Eq. (2) with the input  $A(0, t) = \sqrt{(P_0)}\text{sech}(t/T_0)$ , where  $P_0$  is the peak power of the input pulse, and  $T_0$  is a measure of its width such that the full width at half maximum (FWHM) is  $T_s = 1.76T_0$ . The order  $N$  of a soliton is governed by the relation  $N^2 = \gamma_0 P_0 T_0^2 / |\beta_2|$ . We choose  $T_0 = 20$  fs for an input pulse at the wavelength of 1060 nm. The peak power of the input pulse is selected as  $P_0 = 180$  W to ensure that a fundamental soliton ( $N = 1$ ) is formed inside the fiber.

Figure 1 reveals the dynamic interplay between the higher-order nonlinear and dispersion terms on the shaping of the Raman soliton. Figures 1(b)–(d) compare the spectral evolution of this fundamental soliton for three different forms of  $\gamma(\omega)$ , keeping the GVD profile the same. Figure 1(b) corresponds to the actual nonlinear profile of the PCF (dotted line) shown in (a) and includes terms up to the third-order ( $\gamma_3$ ) in (3); (c) includes only the first-order term [dashed line in (a)] and represents the prediction of conventional GNLS; and (d) assumes that  $\gamma(\omega) = \gamma_0$  and ignores all frequency dependence of the nonlinear parameter (no self-steepening).

In addition to the common qualitative feature of RIFS suppression through spectral recoil from the NSR beyond the second ZDWL [5], we also see significant differences in Figs. 1(b)–(d) produced by different forms of the nonlinearity profile. More specifically, the distance at which the soliton's wavelength approaches the second ZDWL and the NSR is emitted is quite different for the three nonlinearity profiles. For this reason, suppression of the RIFS occurs at different fiber lengths for different  $\gamma(\omega)$ . The rate at which the soliton's wavelength increases is the largest in (d) with the soliton reaching the second ZDWL at a distance of only 13 m. This distance increases to 23 m and 43 m in (c) and (b), respectively. Thus, we can conclude that the standard GNLS overestimates the RIFS

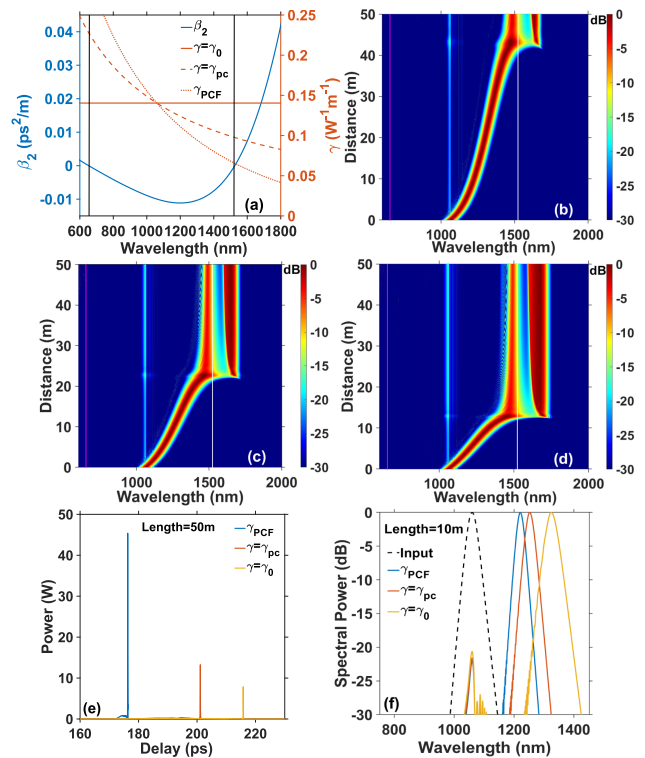


**Fig. 1.** (a) Dispersion (blue) and three nonlinear profiles for a specific PCF [ $\Lambda \approx 1.4$   $\mu\text{m}$  (distance between air holes), core diameter  $\approx 1.30$   $\mu\text{m}$ ]. Vertical lines indicate ZDWLs. Spectral evolution of a soliton ( $N = 1$ ) over 50 m of this PCF for (b) dotted, (c) dashed, and (d) flat nonlinear profiles. Purple and white vertical lines in (b), (c), (d) indicate the first and second ZDWLs. (e) Temporal profiles of the soliton at 50 m in the three preceding cases. (f) Optical spectra at 10 m in three cases compared to the input spectrum.

for most PCFs, and the actual frequency dependence of the nonlinear profile must be used for comparison with experiments performed with such fibers.

As an example, consider an experiment performed in a 50-m-long PCF and the temporal and spectral data recorded at this distance. Figure 1(e) compares the predictions for three nonlinearity profiles by plotting the temporal profile of the fundamental soliton, delayed in time because of its deceleration by the RIFS, at the fiber's output. Different heights of the three peaks indicate clearly that the soliton's energy is quite different in the three cases. In particular, the peak power of the soliton is enhanced by more than a factor of three when we compare the actual frequency dependence of  $\gamma(\omega)$  (blue) with the prediction of its linear approximation (red curve). The yellow curve indicates the most delayed soliton with the least peak power for the frequency independent nonlinear profile.

In Fig. 1(f), we compare the soliton's spectra for three nonlinearity profiles at a distance of 10 m with the input spectrum (dashed black curve). The spectrum is shifted most when  $\gamma$  is treated as being constant, and the smallest shift occurs when we use the actual profile,  $\gamma = \gamma_{\text{PCF}}$ . This feature indicates that the width of the soliton is also different in the three cases when the spectrum becomes close to the second ZDWL [1]. This is the reason that different amounts of energy are lost to the NSR in the three cases. From a practical standpoint, the width, as well as

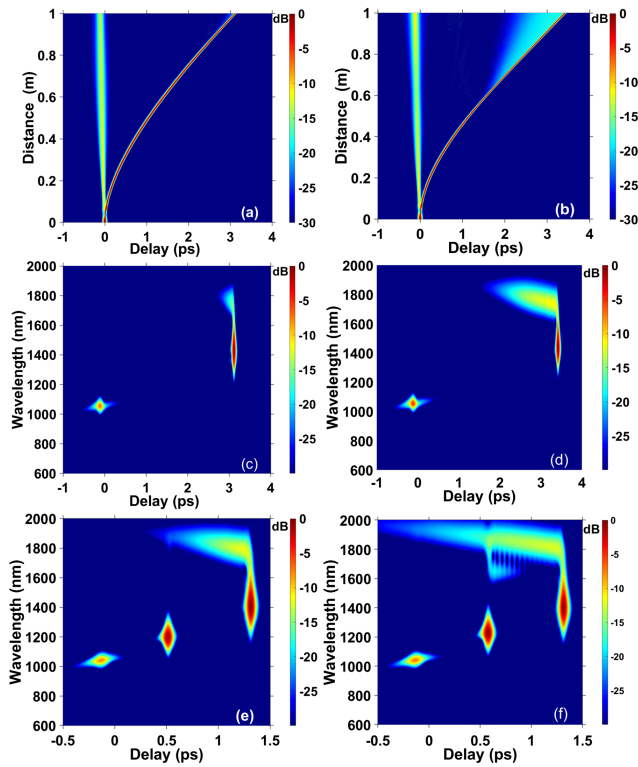


**Fig. 2.** Temporal evolution of a second-order soliton using (a) actual nonlinear profile and (b) its linear approximation. (c), (d) Corresponding spectrograms at 1 m. (e), (f) Spectrograms in the same two cases at 0.4 m for a third-order soliton.

the amplitude of the output pulse can be controlled by tailoring the nonlinearity profile of the PCF used in an experiment.

One may wonder how the preceding evolution scenario changes for higher-order solitons. In this section, we first consider a second-order soliton and choose  $P_0 = 715$  W to ensure  $N = 2$ . Figures 2(a) and (b) show the temporal evolution of this soliton over a distance of 1 m using (a)  $\gamma(\omega) = \gamma_{PCF}$  and (b)  $\gamma(\omega) = \gamma_{pc}$ . As expected, the second-order soliton undergoes fission and splits into two fundamental solitons of different widths [9,22]. This fission occurs at a distance of around 3.5 cm, and the speed of the shortest fundamental soliton is reduced more and more due to an increasing RIFS. We observe in (b) that NSR is emitted starting at a distance of 62 cm. No NSR is seen in (a). To understand this difference better, we show in Figs. 2(c) and (d) the simulated spectrograms at a distance of 1 m. In both cases, we see two fundamental solitons with different spectra. The absence of the NSR in (a) can be solely attributed to the fact that the soliton's wavelength has just reached the second ZDWL at a distance of 1 m. This happens at a shorter distance in (b), resulting in the formation of a dispersive wave. Note that soliton's delays are also slightly different, 3.1 ps in (c) and 3.4 ps in (d).

Next, we increase the peak power to 1.61 kW, resulting in the formation of a third-order soliton ( $N = 3$ ). Figures 2(e) and (f) show the simulated spectrograms at a distance of 0.4 m in the same two cases: (e)  $\gamma(\omega) = \gamma_{PCF}$  and (f)  $\gamma(\omega) = \gamma_{pc}$ . As expected, the third-order soliton has split into three fundamental solitons with different widths and different spectra. A dispersive wave forms in both cases when the soliton's wavelength becomes close to the second ZDWL, but it is much less

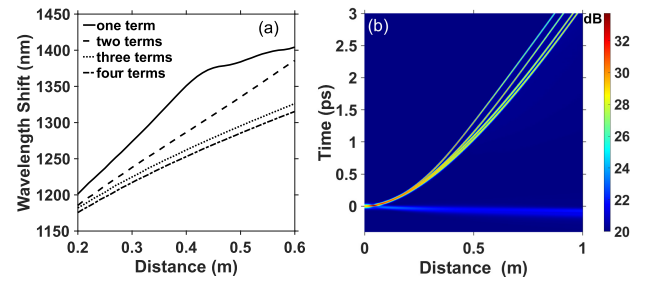


**Fig. 3.** (a) Wavelength shift (RIFS) as a function of distance for a second-order soliton when terms up to fourth order are included in the Taylor expansion of  $\gamma(\omega)$ . (b) Temporal evolution of the soliton in the same four cases.

**Table 1. Values of the Four Coefficients Obtained by Fitting  $\gamma_{PCF}$  to a Cubic Polynomial**

$$\begin{aligned}\gamma_0 &= 0.1402 \text{ W}^{-1} \text{ m}^{-1} \\ \gamma_1 &= 1.412 \times 10^{-1} \text{ W}^{-1} \text{ m}^{-1} \text{ fs} \\ \gamma_2 &= 1.3033 \times 10^{-5} \text{ W}^{-1} \text{ m}^{-1} \text{ fs}^2 \\ \gamma_3 &= -1.5185 \times 10^{-8} \text{ W}^{-1} \text{ m}^{-1} \text{ fs}^3\end{aligned}$$

intense and much less spread in (e) because of a reduced rate of the RIFS of the soliton. Interestingly, there is an additional spectral feature around 1620 nm in (f). This feature results from the trapping of the NSR by the middle soliton [23,24]. A fraction of NSR energy released by the shortest soliton is trapped by the middle soliton because of their temporal overlap and its spectrum shifts toward the blue side through cross-phase modulation. This does not occur in (e) because of the reduced spreading of the dispersive wave. It is important to stress that the frequency dependence of the nonlinearity plays a pivotal role in controlling the trajectory of both the soliton and the NSR.

An important question is how many terms should be retained in the Taylor expansion of  $\gamma(\omega)$  given in Eq. (3). In Fig. 3(a), we show how the wavelength of a second-order soliton changes with distance inside the fiber when the number of terms in this expansion is increased from one to four. When only the first term is included,  $\gamma$  becomes a constant with no frequency dependence. In this case (solid line), wavelength first increases linearly with distance, as expected from theory, and then begins to saturate after 0.43 m because of the onset of the RIFS suppression, as discussed earlier. When the linear  $\gamma_1$  term is included, saturation of the RIFS stops because of the reduced slope of the dashed line in Fig. 3(a). The inclusion of  $\gamma_2$  (dotted line) and  $\gamma_3$  (dashed-dotted line) reduces this slope further and also makes the RIFS increase sublinear. We have found that the RIFS does not change much as more terms are included, indicating that the nonlinear profile can be well approximated with a cubic polynomial. The values of the four coefficients for the cubic polynomial fitted to the  $\gamma_{PCF}$  for a specific PCF are given in Table 1.

The temporal delay of the soliton induced by the wavelength shift is plotted for the same four cases in Fig. 3(b). This delay is a result of the reduction in the soliton's speed because of its changing wavelength. The resulting temporal delay of the soliton does not increase linearly with distance, even when the wavelength itself increases linearly. Note that NSR cannot be seen in (b) because of a reduced range of the amplitude scale shown on the right. The smallest delay occurs when all four terms are included in the Taylor expansion so that  $\gamma(\omega) = \gamma_{PCF}$ .

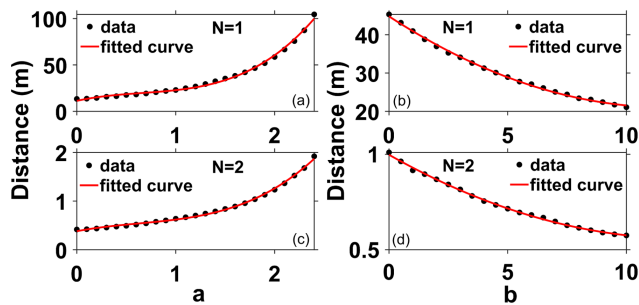


**Fig. 4.** Distance at which the RIFS is fully suppressed is plotted as a function of  $a$  (left) and  $b$  (right) for a fundamental soliton (top row) and a second-order soliton (bottom row).

The suppression of RIFS occurs for any PCF with two ZDWLs [5]. To understand how this suppression depends on parameters  $\gamma_1$  and  $\gamma_2$ , we introduce their dimensionless versions  $a$  and  $b$  by writing the frequency dependence of the nonlinearity in the form  $\gamma(\omega) = \gamma_0(1 + a(\omega - \omega_0)/\omega_0 + b(\omega - \omega_0)^2/2\omega_0^2)$ , where  $a = \gamma_1\omega_0/\gamma_0$  and  $b = \gamma_2\omega_0^2/\gamma_0$ . At the input wavelength of 1060 nm, we find  $a = 1.7903$  and  $b = 0.2936$  for the PCF used in this work. However, these values will change for other PCFs. We note that it has been common in the past to use the values  $a = 1$  and  $b = 0$ , which correspond to the self-steepening case. In Fig. 4, we vary these two parameters to study how the distance at which the RIFS is suppressed depends on their values. The top and bottom rows correspond to  $N = 1$  and 2, respectively. In (a) and (c), we vary  $a$ , keeping  $b = 0$  fixed. In (b) and (d), we vary  $b$ , keeping  $a = 1.8$  fixed.

Several features of Fig. 4 are noteworthy. The length scale is reduced by a factor of 50 when we switch from  $N = 1$  to  $N = 2$  soliton. The lowest order fit that matches the simulation points (data) is cubic for (a) and (c) and quadratic for (b) and (d). A salient feature is that the nature of the curve is opposite for increasing  $a$  and  $b$ . The main reason behind this trend is the RIFS of the soliton towards the second ZDWL. The rate of RIFS decreases with increasing  $a$  but increases with  $b$ . As a result, it takes a longer length in the first case and a shorter length in the second case to reach the second ZDWL. Note that  $b$  is varied over a wide range such that  $0 < b < 10$ . This range can be realized in practice by doping the fiber with nanoparticles made of gold [15].

Although we used a PCF as an example to emphasize the role of the frequency dependence of the nonlinear parameter on the evolution of short solitons, our conclusions should apply to any high-confinement optical waveguide, including tapered fibers and suspended-core fibers. The frequency dependence of  $\gamma(\omega)$  in such fibers cannot be replicated using the conventional GNLS based on the self-steepening effect and includes only the first order in a Taylor expansion. To ensure the conservation of the photon number, we used the recently proposed modified GNLS to reveal the importance of few-cycle solitons in a nonlinear waveguide. Our numerical simulations reveal that the rate of RIFS (along the fiber's length) is influenced by higher-order

nonlinear terms, in addition to third-order dispersion and self-steepening. These terms also control the shedding of dispersive radiation close to the second ZDWL of the fiber. For the specific PCF design used in this work, the RIFS of the soliton is reduced compared to the self-steepening case often used in literature, which in turn affects the temporal delay of the soliton. The peak power of the soliton is also affected close to the second ZDWL of the fiber owing to a reduction in the amount of dispersive radiation. These features are important when solitons are used to design a wavelength-tunable optical source.

**Funding.** Cluster of Excellence QuantumFrontiers (EXC 2123, Project No. 390837967); Deutsche Forschungsgemeinschaft within the Cluster of Excellence PhoenixD (Photonics, Optics, and Engineering–Innovation Across Disciplines) (EXC 2122 Project No. 390833453); National Science Foundation (ECCS-1933328).

**Disclosures.** The authors declare no conflicts of interest.

**Data Availability.** Data underlying the results presented in this paper are not publicly available at this time but may be obtained from the authors upon reasonable request.

## REFERENCES

- G. P. Agrawal, *Nonlinear Fiber Optics*, 6th ed. (Academic, 2019).
- G. P. Agrawal, *Applications of Nonlinear Fiber Optics*, 3rd ed. (Academic, 2020).
- J. P. Gordon, *Opt. Lett.* **11**, 662 (1986).
- P. Russell, *Science* **299**, 358 (2003).
- D. Skryabin, F. Luan, J. Knight, and P. St. J. Russell, *Science* **301**, 1705 (2003).
- N. Akhmediev and M. Karlsson, *Phys. Rev. A* **51**, 2602 (1995).
- J. R. de Oliveira, M. A. de Moura, J. M. Hickmann, and A. S. L. Gomes, *J. Opt. Soc. Am. B* **9**, 2025 (1992).
- R. Kormokar, M. H. M. Shamim, and M. Rochette, *J. Opt. Soc. Am. B* **38**, 466 (2021).
- J. M. Dudley, G. Genty, and S. Coen, *Rev. Mod. Phys.* **78**, 1135 (2006).
- Q. Lin and G. P. Agrawal, *Opt. Lett.* **31**, 3086 (2006).
- J. Laegsgaard, *Opt. Express* **15**, 16110 (2007).
- K. J. Blow and D. Wood, *IEEE J. Quantum Electron.* **25**, 2665 (1989).
- J. Bonetti, N. Linale, A. D. Sánchez, S. M. Hernández, P. I. Fierens, and D. F. Grosz, *J. Opt. Soc. Am. B* **37**, 445 (2020).
- N. Linale, J. Bonetti, A. D. Sánchez, S. M. Hernández, P. I. Fierens, and D. F. Grosz, *Opt. Lett.* **45**, 2498 (2020).
- A. D. Sánchez, N. Linale, J. Bonetti, and D. F. Grosz, *Opt. Lett.* **45**, 3119 (2020).
- N. Linale, P. I. Fierens, J. Bonetti, A. D. Sánchez, S. M. Hernández, and D. F. Grosz, *Opt. Lett.* **45**, 4535 (2020).
- N. Linale, P. I. Fierens, and D. F. Grosz, *IEEE J. Quantum Electron.* **57**, 6100108 (2021).
- N. Linale, J. Bonetti, P. I. Fierens, S. M. Hernández, and D. F. Grosz, *IEEE J. Quantum Electron.* **57**, 6800207 (2021).
- S. M. Hernández, J. Bonetti, N. Linale, D. F. Grosz, and P. I. Fierens, *Waves Random Complex Media* (2020), pp. 1–17.
- J. Hult, *J. Lightwave Technol.* **25**, 3770 (2007).
- S. Bose, P. H. Reddy, J. Fan, A. Demircan, A. Ruehl, U. Morgner, S. Roy, M. Pal, S. K. Bhadra, and D. Ghosh, *Appl. Opt.* **59**, 9015 (2020).
- A. Husakou and J. Herrmann, *Phys. Rev. Lett.* **87**, 203901 (2001).
- N. Nishizawa and T. Goto, *Opt. Lett.* **27**, 152 (2002).
- A. Demircan, S. Amiranashvili, and G. Steinmeyer, *Phys. Rev. Lett.* **106**, 163901 (2011).